Direct Injection of Aluminum-Organic Matter Flocs to Reduce Soil Permeability and Create a Vertical Flow Barrier in Situ

Zhou, Jianchao; Laumann, S.; Heimovaara, T. J.

Citation (APA)
Zhou, J., Laumann, S., & Heimovaara, T. J. (2022). Direct Injection of Aluminum-Organic Matter Flocs to Reduce Soil Permeability and Create a Vertical Flow Barrier in Situ. *Journal of Geotechnical and Geoenvironmental Engineering*, *148*(11), Article 04022095-1. https://doi.org/10.1061/(ASCE)GT.1943-5606.0002886

Important note
To cite this publication, please use the final published version (if applicable).
Please check the document version above.

ASCE

Direct Injection of Aluminum–Organic Matter Flocs to Reduce Soil Permeability and Create a Vertical Flow Barrier In Situ

J. Zhou[1]; S. Laumann[2]; and T. J. Heimovaara[3]

Abstract: This study presents a novel geotechnical engineering approach that utilizes naturally occurring processes to reduce soil permeability in-situ. This approach is inspired by a soil stratification process (Podzolization), where a low permeability layer is formed by metal-organic matter precipitates. In a field experiment, a direct aluminum-organic matter (Al-OM) floc injection was applied to create a continuous vertical flow barrier in a dike. Direct injection uses the shear-dependent size of Al-OM flocs. High-shear conditions (i.e., during injection) lead to the breakage of Al-OM flocs and thus allow their transportation in soils. When the injection stops and low-shear conditions prevail, the Al-OM flocs re-grow in size and block the pores, which ultimately reduces soil permeability. Two different Al-OM floc concentrations were applied in the field. Results show that a continuous flow barrier is only formed at lower concentrations; at higher concentrations a scattered permeability reduction was achieved. This demonstrates the viability of this approach in reducing soil permeability in-situ and shows that the spatial distribution of the flocs depends on input concentration. **DOI: [10.1061/(ASCE)GT.1943-5606.0002886](https://doi.org/10.1061/(ASCE)GT.1943-5606.0002886).** *This work is made available under the terms of the Creative Commons Attribution 4.0 International license, https://creativecommons.org/licenses/by/4.0/.*

Introduction

The permeability of a soil is a crucial property that controls groundwater flow in the subsurface. Highly permeable soil layers often lead to high seepage flow and can cause a variety of problems, from the spreading of contaminants (Bayer et al. 2004) to excessive uplift pressure underneath dikes (Yihdego 2016), or slope instability (Papagianakis and Fredlund 1984). A solution to these problems lies in the reduction of the soil permeability. Techniques like jet grouting, colloidal-silica injection, and the installation of sheet-pile walls have been successfully applied to reduce soil permeability in many cases (Mulligan et al. 2001; Shen et al. 2004; Nikbakhtan and Osanloo 2009). Many of these traditional approaches, however, face challenges with respect to their environmental impact, as well as high energy and labor costs (Suer et al. 2009). So there is a demand for alternative engineering solutions that are both economically effective and have a minimal environmental impact. We developed a nature-based geo-engineering technique to reduce soil permeability that was inspired by the soil stratification process called Podzolization. During Podzolization, precipitation and accumulation of organo-metallic precipitates result in a distinct soil horizon that can have a significantly reduced permeability (Sauer et al. 2007).

One of the challenges for innovative nature-based geo-engineering techniques is upscaling the process from the laboratory to the field scale (DeJong et al. 2013; Proto et al. 2016). Doing experiments at the field scale is essential (van Paassen 2011). A bio-based geo-engineering solution based on microbially induced calcite precipitation (MICP) to modify soil properties, such as reducing soil permeability (Blauw et al. 2009), was developed about a decade ago. Although the MICP concept has been studied extensively in laboratory experiments at the bench scale and with numerical models (DeJong et al. 2010, 2013; van Wijngaarden et al. 2016), to our knowledge only a few field-scale applications of this biosealing technique have been reported (Ivanov and Chu 2008; DeJong et al. 2010). A pilot project using the biosealing principle was carried out in 2009 in order to construct a flow barrier to stop seepage underneath a dam along the River Danube in Austria (Blauw et al. 2009; van Paassen 2011). Although it was reported that the seepage was reduced by a factor of 10 four to five months after the field injection practice, little information on the experimental set-up, field data acquisition system, and data processing method can be found. This makes it hard for other researchers to benefit from this project. In addition to soil permeability reduction, the MICP concept can also be applied to strengthen soil mechanical properties. More field experiments that use MICP for ground improvement have been reported (Haouzi and Courcelles 2018). However, many of these applications are surficial applications [i.e., mitigation of surface erosion of loose sand (Gomez et al. 2015), or reinforcement of an aboveground soil retaining wall structure (Haouzi and Courcelles 2018)] at relatively small scales, i.e., the treatment zone in the soil retaining wall is 3 m height and 6 m length. In-situ large-scale application of nature-based geo-engineering techniques for soil permeability reduction, particularly at depth, are hard to find.

Organo-metallic precipitates occur as floc-like structures (Scheel et al. 2008) and consist in our case of aluminum (Al) and organic matter (OM). Al-OM flocs are several hundred micrometers in size (Wang et al. 2009; Yu et al. 2010), which is significantly larger than the pore size in many soils (DeJong et al. 2010). Due to their large size, these flocs are filtered from the system after

[1]Formerly, Ph.D. Student, Faculty of Civil Engineering and Geosciences, Delft Univ. of Technology, 23 Stevinweg 1, 2628 CN, Delft, Netherlands (corresponding author). ORCID: https://orcid.org/0000-0001-5207-3023. Email: j.zhou-3@tudelft.nl

[2]Research Manager, Faculty of Civil Engineering and Geosciences, Delft Univ. of Technology, 23 Stevinweg 1, 2628 CN, Delft, Netherlands; formerly, Expert Advisor, Tauw BV, Handelskade 37, 7417 DE, Deventer, Netherlands. Email: S.J.Laumann@tudelft.nl

[3]Professor, Faculty of Civil Engineering and Geosciences, Delft Univ. of Technology, 23 Stevinweg 1, 2628 CN, Delft, Netherlands. Email: t.j.heimovaara@tudelft.nl

© ASCE 04022095-1 J. Geotech. Geoenviron. Eng.

J. Geotech. Geoenviron. Eng., 2022, 148(11): 04022095

formation and as a consequence, reduce the permeability (Ryan and Elimelech 1996). This newly developed technique was applied in a field experiment for the first time by Zhou et al. (2019). In that case study, the in-situ precipitation of Al-OM flocs was induced by separate injection of Al and OM solutions into the subsurface. The results show that the in-situ production of Al-OM flocs can reduce soil permeability up to a factor of about 50 (Zhou et al. 2019). It was, however, also concluded that in-situ mixing and reaction of Al and OM is not very efficient, because not all material injected in to the soil led to the formation of flocs. In addition, the reliance on in-situ mixing and reaction required a relatively long field injection duration in order to maintain the production of Al-OM flocs in-situ. Field installation for injection wells, in which case are needed for both components, had to be carried out, as well. As a result, this makes this solution less economically attractive, particularly for large-scale applications.

In this study we present an alternative approach that originated from detailed analysis of the Zhou et al. (2019) field test, and is based on ex-situ production of Al-OM flocs, followed by the injection of a floc suspension. This has a significant engineering advantage, because in-situ mixing and reaction is no longer required. The direct injection of Al-OM flocs makes use of the fact that the size of the flocs is shear-dependent, which is well established in the water treatment literature (Li et al. 2006; Jarvis et al. 2006; Yu et al. 2010). Under high shear conditions, flocs break into colloids that are in the low μm range (Wang et al. 2009). Flocs of this size can be transported through a porous medium (Wiesner et al. 1996; DeJong et al. 2010; Syngouna and Chrysikopoulos 2012). Floc size and transport can be controlled by manipulating the flow field, because the shear is linearly correlated to the Darcy flow velocity (Tosco and Sethi 2010). Injection usually creates a radial flow field, where the flow velocity deceases significantly with radial distance from the injection point (Tosco et al. 2014). This means that the Al-OM flocs are mobile in the close vicinity of the injection point, where a sufficiently high flow velocity is achieved. As soon as low-shear conditions prevail, i.e., at larger radial distances from the injection point or after injection has ceased, the Al-OM flocs re-grow in size and subsequently deposit in the porous medium.

We applied this direct Al-OM floc injection technique for the first time in a full-scale field experiment at a dike that surrounds a water reservoir in the Netherlands. During the experiment, Al-OM flocs were prepared on site and injected into the dike body using direct-push injection. The aim of this field was to create a 70 m long vertical flow barrier with a height of 7 m in the dike body by reducing the local soil permeability. The flow barrier is expected to reduce the groundwater flow, which leads to a head drop at its location. According to Darcy's law the magnitude of this head drop is linear to the permeability of the flow barrier if the background flow rate stays constant. The effectiveness of the flow barrier in reducing groundwater flow, however, is not only dependent on its permeability but also on its continuity (Yihdego 2016). As stated in our previous study (Zhou et al. 2019), gaps within the flow barrier will lead to the occurrence of preferential flow and diminish the effectiveness of the barrier. This has a large consequence on the quantification of the permeability reduction, as a discontinuity may result in unchanged hydraulic signals despite the locally reduced soil permeability.

This experiment was part of a research program aiming to assess the feasibility of direct injection of Al-OM flocs to reduce soil permeability and to quantify the achieved reduction in permeability. Doing the experiment at full-scale also gave the opportunity to study the spatial distribution of the reduction in permeability. In this paper we compare the results obtained from two different injection scenarios, where the recipe to produce the Al-OM flocs was varied.

In order to determine the hydraulic characteristics of the site before, during and after the experiment, monitoring wells were installed and used to perform field hydraulic tests. Monitoring data are analyzed together with simulation results that re generated by a site-specific groundwater flow model.

Materials and Methods

Site Description

The field site is part of an 8 km long dike that surrounds the de Gijster water reservoir in the Biesbosch (Fig. S3), of which the construction was finalized in 1979. The dike was built on top of the former ground surface [1 m NAP (Dutch reference system)] up to a height of 9.5 m NAP using medium to coarse sand that was available during the reservoir construction. Information on the grain size distribution of the sand can be found in the Supplemental Materials (i.e., Fig. S4). Site investigation revealed that the soil layer underneath the dike consists of fine to medium sand that reaches a depth of approximately −3.5 m NAP, and which is underlain by a peat layer of varying thickness (up to 1.5 m) [illustrated in Fig. 1(a)]. Soil profiles, recorded from the field installation, are provided in Fig. S1. The pilot site covers a surface area of 1,260 m² and is located at the east side of the water reservoir. At this point excessive seepage flow occurs, which leads to fully saturated soil conditions at the toe of the dike. The high water content does not raise any concerns regarding dike stability, but does result in high maintenance costs due to muddy conditions and a limited bearing capacity of the top soil.

The water level in the reservoir is usually maintained at 6.50 m NAP, while the water level in the adjacent ditch, at a distance of about 50 m from the reservoir, fluctuates around 0.40 m NAP. At the reservoir side, the dike is sealed under the former ground surface by asphalt and clay. Due to this surface sealing, the hydraulic head measured in the middle of the dike ranges between 2.20 and 2.80 m NAP. During the field experiment (in the summer of 2018) the hydraulic boundary conditions changed, due to dredging activities in the reservoir basin, which started in the same period as our field experiment. During the dredging work, parts of the former top soil that were still present in the basin were removed in order to adapt the profile of the water reservoir so that it meets the original design criteria, which was to excavate a water reservoir with a smooth slope [Fig. 1(a)].

Design and Implementation of the Field Experiment

A site-specific groundwater flow model (described in later text) was developed in order to determine the reason for the high water content at the toe of the dike. This analysis confirmed that the excessive seepage originates from the water reservoir where water infiltrates the sand layers above the peat layer and is transported towards the ditch [Fig. 1(a)]. A measure to reduce the water content of the soil at the toe of the dike is to create an up-gradient vertical flow barrier that covers the entire transport path of the seepage. The flow barrier lowers the groundwater table in its downstream direction and also reduces the groundwater discharge rate (Anderson and Mesa 2006). As a consequence, the top soil will become drier, which reduces the maintenance effort at the site.

The design of the flow barrier is based on a scenario analysis using a site-specific flow model. The permeability reduction that is induced by the Al-OM flocs is set to 50 times, based on previous experiments (Zhou et al. 2019). According to the simulation results, a sufficiently lowered groundwater table at the toe of the dike requires the flow barrier to be at least 1 m thick. In order to prevent

© ASCE 04022095-2 J. Geotech. Geoenviron. Eng.

J. Geotech. Geoenviron. Eng., 2022, 148(11): 04022095
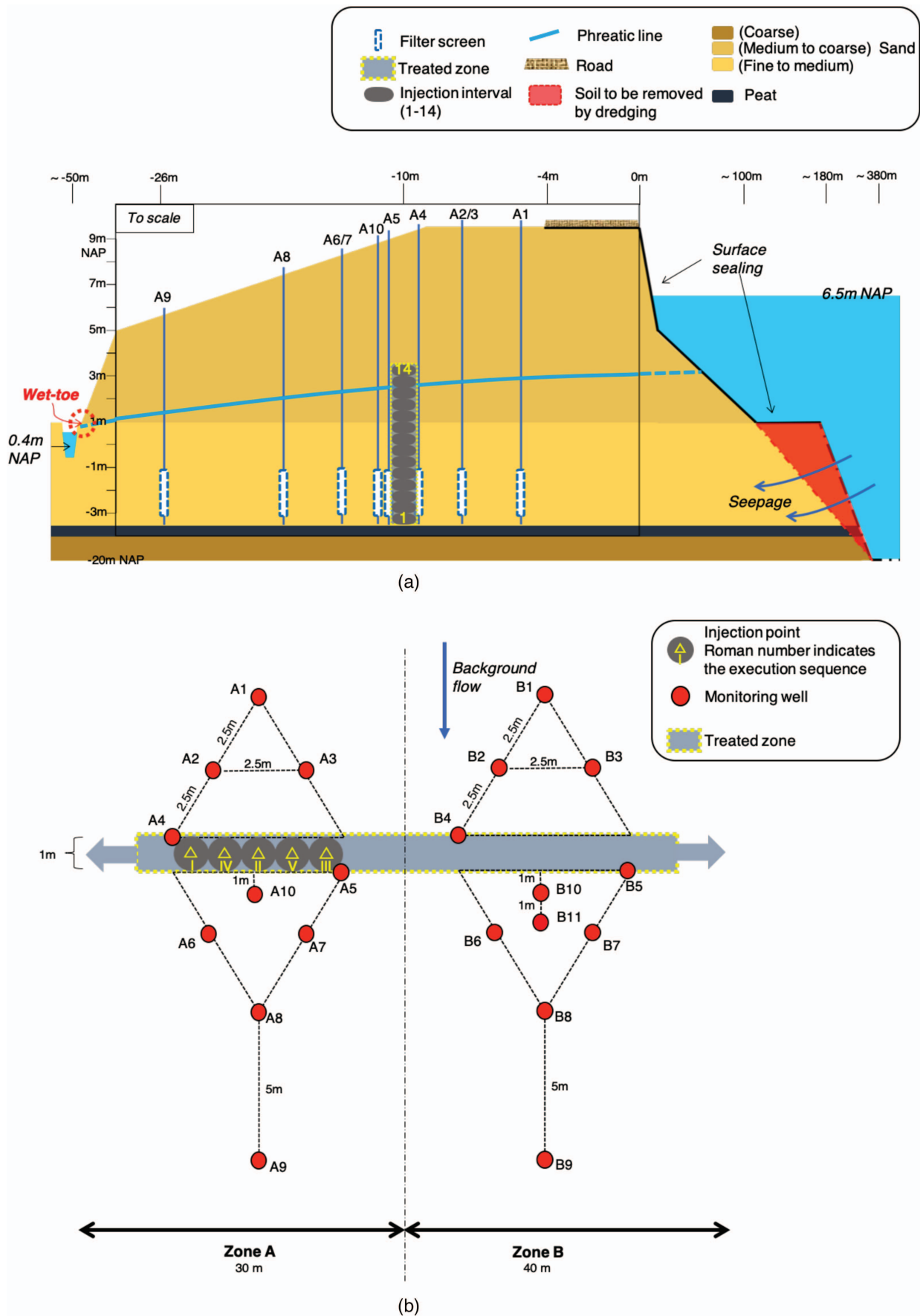
Fig. 1. (Color) Illustration of the site: (a) profile view (only a section of this figure is plotted to scale); and (b) top view. An example of the injection sequence is illustrated in (b).

vertical overflow, the barrier needs to be higher than the current groundwater table. We designed the height of the flow barrier to be 7 m [5–12 m below ground surface (bgs)], where 1.5 m extends above the original water table in the dike [Fig. 1(a)]. The pilot area is 70 m long and the implementation was carried out parallel to the dike structure at 10 m distance from the top of the dike (Fig. 1). According to the simulation results and existing literature (Hudak 2001; Anderson and Mesa 2006), the dewatering effect of a finite flow barrier decreases as the down-gradient distance increases, which would make a location closer to the toe of the dike the preferred option. However, this is not feasible due to the limitations of the machine used to inject the flocs, and the slope of the dike.

The machine (MDE Drive, Heijmans bv, Rosmalen, Netherlands) is equipped with a direct-push system and uses an injection rod (33 mm diameter and 20 cm long) with four annular distributed injection ports for the injection of the Al-OM floc suspension. A picture of the machine and the setup of the equipment is given in Fig. S5. The injection location, depth, rate, and duration were programmed beforehand and recorded continuously. The radius of influence (ROI) of the Al-OM flocs was targeted at 0.5 m. Assuming full displacement of groundwater [expressed in Eq. (1); (Payne et al. 2008; Luna et al. 2015)] and a safety margin of 10%, the injection volume for the 7 m high barrier at each injection point should be 1.82 m^3 (1.1 pore volume). With a ROI of 0.5 m, 70 injections are needed to complete the 70 m long flow barrier

$$PV = \varepsilon_p \cdot \pi \cdot ROI^2 \cdot L_s \qquad (1)$$

where PV is the pore volume of the aquifer $[L^3]$; ε_p is the porosity $[L^3/L^3]$ (assumed to be 0.3, based on the characteristics of the sand); and L_s is the length of the well screen $[L]$, which in this study is equivalent to the height of the flow barrier.

In order to create a 7 m high flow barrier with the direct-push system, the injection at each injection point was divided into 14 intervals of 0.5 m. This execution routine is considered favorable for a uniform distribution of Al-OM flocs (Luna et al. 2015). The injection rod was first pushed down to 11.75 m bgs, followed by the first injection interval [illustrated in Fig. 1(a)]. After injecting 0.13 m^3 of Al-OM floc suspension at a rate of 60 m^3/d, the injection rod was lifted by 0.5 m for the following interval. A target volume of 1.82 m^3 was injected throughout the 14 intervals at each injection point. The injection sequence was designed to minimize the impact of ongoing injection on the earlier-injected Al-OM flocs. In order to guarantee that the injected Al-OM flocs have sufficient time to re-grow and deposit [which takes not longer than a few minutes, according to the literature (Wang et al. 2002, 2009; Zhao et al. 2011)], a back and forth injection pattern was implemented [illustrated in Fig. 1(b)], ensuring that no neighboring injections were implemented sequentially in time.

In order to test two injection scenarios, the field site was subdivided in two zones, where different Al-OM floc concentrations were applied. An OM input concentration of 3 g/l was applied in Zone A (30 m long), and a 5 g/l OM input was used in Zone B (40 m long). The Al-OM floc suspension was prepared daily on site, by mixing aluminum chloride (AlCl$_3 \cdot$ 6H$_2$O, Alfa Aesar, Germany) with OM (HUMIN P775, Humintech, Germany) in a continuously stirred reactor (volume of 9 m^3). Water for preparing the suspension was taken from the reservoir, and its pH was around 7.5, with an electrical conductivity (EC) of approximately 0.5 ms/cm. Jansen et al. (2002) demonstrated that insoluble Al-OM flocs are formed when the molar metal to carbon (M/C) ratio is above certain threshold. In this experiment, Al-OM flocs were formed as soon as the molar M/C ratio was above 0.05, using the water extracted from the reservoir. The appearance of flocs was inspected daily by taking a small sample before the injection

started. The sample was left still for a short period of time, after which visual inspection was performed to check whether segregation of the sample occurred; i.e., whether the flocs settled to the bottom if they formed. During a period of 10 working days, 54.6 and 72.8 m^3 of the Al-OM floc suspension was injected in Zones A and B, respectively. This corresponds to a total injected mass of around 49.2 kg aluminum salt and 163.8 kg OM in Zone A, and 116.4 and 354 kg of the two components in Zone B. The injection went smoothly and without any major difficulties.

Laboratory Observations

Batch Experiment
To characterize the Al-OM flocs as a function of applied shear rate, 100 mg/l OM solution was mixed with an Al solution to create a Al-OM floc suspension, and the size of the flocs was analyzed by laser diffraction (Malvern Mastersizer 2000, Malvern Instruments, UK) at three stirring speeds: 150, 300, and 450 rpm. For determining the floc size using laser diffraction, no higher OM input concentration was possible. The variability of the Al-OM floc size is depicted in Fig. S6, together with the size of the original OM. Size characterization of the OM by laser diffraction revealed a bimodal distribution with two distinct peaks around 0.17 and 19.35 μm (d10/d50/d90 = 0.09/0.17/14.12 μm). The Al-OM flocs have a monomodal distribution and the size decreases with increasing steering speed, from 606 μm (150 rpm; d10/d90 = 220/1,204 μm), to 221 μm (300 rpm; d10/d50/d90 = 89/221/447 μm), and 104 μm (450 rpm; d10/d90 = 44/210 μm). This is in line with previous research showing that the floc size distribution and the associated growth and breakage of flocs is depending on the applied shear rate (Jarvis et al. 2006).

1D Column Experiments
Prior to the field experiment, 1D column experiments were carried out in the lab to study the effectiveness of injected Al-OM floc suspension in reducing soil permeability. In these column experiments, an Al-OM floc suspension was injected into the sand column at a constant flow velocity, where injection flow velocity (ranging from 12.6 to 66.7 m/d) or input OM concentration (ranging from 0.1 to 5 g/l) varied. Because the shear is linearly correlated to the Darcy flow velocity (Tosco and Sethi 2010), the varied injection flow velocity was designed to simulate different shear conditions. Details about the experimental set-up and testing procedure are provided in the Supplemental Materials.

The column was equipped with five pressure sensors installed at different levels [Fig. 2(a)] in order to quantify the distribution of reduction in permeability over time. This is essential because, under the 1D column condition, the flow velocity throughout the entire sand column stayed constant, while the field injection would create a radial flow field in which the flow velocity decays at larger radial distances. The 1D column experiments showed that Al-OM flocs deposit in high amounts close to the inlet and in decreasing amounts further downstream. The experiments also demonstrated that at a higher flow velocity the transport distance of Al-OM flocs in sand increases [Fig. 2(b)]. This can be attributed to the shear-dependency of the floc size, where high flow velocity creates high shear conditions that break injected flocs into smaller sizes. Smaller flocs can be transported for longer distances in porous media (Ryan and Elimelech 1996). Apart from the flow velocity, another set of column tests with varying input OM concentrations revealed that the input concentration also has an impact on the transport distance of the Al-OM flocs. The volume of soil impacted by flocs at an OM input concentration of 5 g/l is 68% of the volume impacted at a concentration of 3 g/l, and 47% of that at 1 g/l. This is again
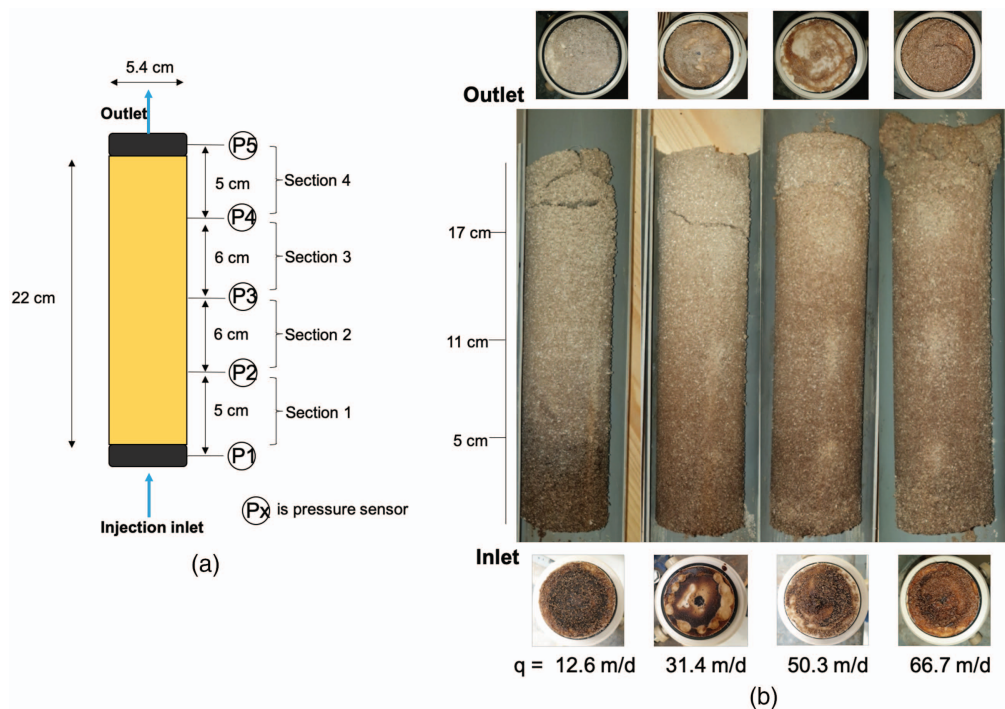
Fig. 2. (Color) Schematic illustration of (a) the experiment set-up; and (b) a graphical comparison of the transport distance of flocs as a function of injection velocity.

in line with particle/colloid transport theory, where the deposition rate of particles correlates with particle concentration: A higher concentration leads to more profound deposition, which limits the transport distance of flocs in porous media (Tosco and Sethi 2010; Syngouna and Chrysikopoulos 2012).

Regarding permeability reduction, the hydraulic conductivity reduction (HCR) derived from the pressure sensors data (Fig. 3) showed that permeability reduction is correlated with the mass of deposited Al-OM flocs, which was qualitatively determined based on the color of the sand: Greater darkness corresponds to a larger amount of deposited Al-OM flocs [Fig. 2(b)]. Because the rheological properties of the Al-OM floc suspension are nearly identical to that of water, the reduction in hydraulic conductivity is caused by a reduction in the soil's permeability. Significant reduction in permeability (i.e., more than 500 times) was measured close to the injection inlet, while in the top of the sample (far from the inlet) the presence of Al-OM flocs was negligible, with little to no reduction in permeability.

Fig. 3 gives the results for an experiment carried out at a flow velocity of 31.4 m/d, where flocs were injected at a concentration of 1 g/l. After injecting 10 pore volume of floc suspension (approximately 2 l), the flow was stopped for 1 h. After this resting period the flow was restarted at 3.2 m/d to measure the final permeability state of the sample. In the Supplemental Materials we present results for the experiments carried out at the higher flow rates of 50.3 and 66.7 m/d.

The results in Fig. 3(a) clearly show the decrease in HCR with height along the column. Fig. 3(b) shows the HCR of the bottom section of the column, and of the total column, related to the total mass of flocs injected into the column. The HCR initially increases in an exponential fashion until it slowly reaches a plateau value. This fits well with filtration theory (Ryan and Elimelech 1996; Syngouna and Chrysikopoulos 2012), where Al-OM flocs initially cover the pore throats, which is an effective permeability reduction mechanism. In time, further deposition fills the pore space, and this

is a less effective mechanism for reducing permeability. Because the majority of flocs was filtered in the bottom section, the mass as well as the size of the flocs were decreasing in the further downstream sections. As a result, the HCR of other sections [i.e., Sections 2 and 3 in Fig. 3(a)] shows a gradual increase rather than the exponential increase observed in the bottom section. Clearly, the injection led to a layered system with varying permeability along the direction of the injection flow. Therefore, the average permeability of the entire column is the harmonic mean of all layers, and is more sensitive to the lowest permeability among these layers. This is why the trend of average HCR trails that of section 1, though with a reduced magnitude [Fig. 3(b)].

After the resting period the permeability of the sand column clearly shows that the permeability has further reduced because of the increase in floc size due to regrowth [Fig. 3(a)].

Monitoring and Data Analysis

In total, 21 monitoring wells (50 mm outer diameter) were installed (illustrated in Fig. 1) in the middle of both Zones A (10 wells) and B (11 wells). The spatial distribution of each monitoring system consists of two triangles that are mirrored with respect to the injection line. This was intended to enable understanding the effect of the background flow on the field injection, as the background flow direction is perpendicular to the orientation of the injection line [Fig. 1(b)]. At the down-gradient side of the injection line, additional wells were installed to monitor the hydraulic head on-site. The filter screen of each well (2 m long) was placed at approximately −3 to −1 m NAP, which is 0.5 m above the peat layer [Fig. 1(a)].

Monitoring at the site was carried out using 17 pressure, EC, and temperature sensors (CTD sensors; Van Essen Instruments, Delft, Netherlands). These were used to monitor the changes in hydraulic head and EC on site. The time interval for measurement and the location of the divers were varied depending on the field activities:
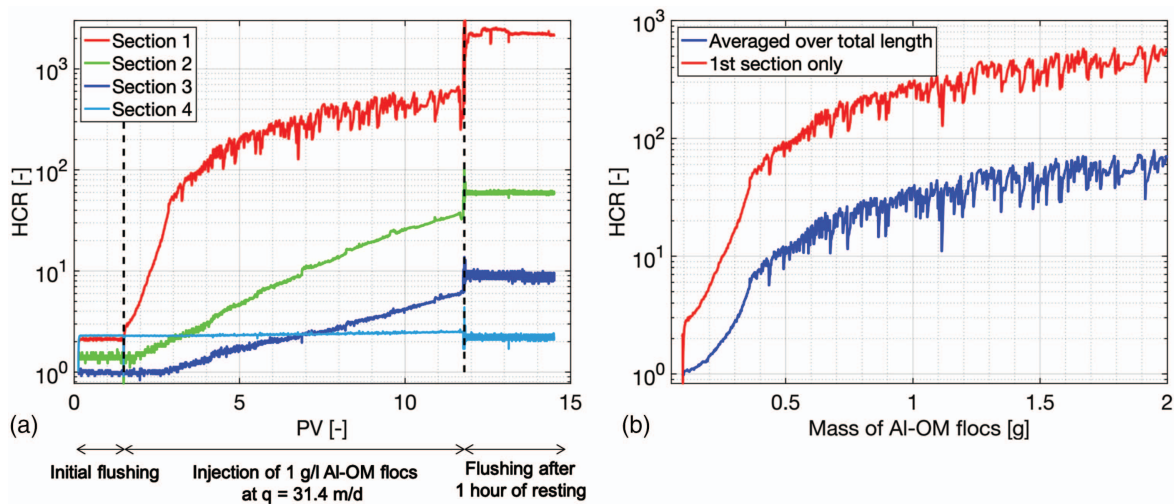
Fig. 3. (Color) Hydraulic conductivity reduction (a) at different sections over PV at the injection velocity of 31.4 m/d; and (b) the correlation between mass of injected Al-OM flocs versus the achieved reduction in hydraulic conductivity at the lowest section (marked in red) and averaged over the entire column (in blue).

When monitoring the natural hydraulic gradient, the time interval was set to 10 mins, and the locations of the divers were switched bi-weekly to ensure complete coverage of all wells; during injection and pumping tests, the time interval was shortened to 10 s and full coverage of all wells was ensured in the monitored zone.

In order to characterize the hydraulic properties of the site and understand the impact of the injection, constant-rate pumping tests, with a pumping rate of around 30 m³/d, were performed in Wells A9 and B9 before, immediately after, and three months after the injection. We applied Dupuit-Thiem's solution [Eq. (2); (Pinder and Celia 2006)] in order to estimate the hydraulic conductivity of the site from the pumping test data

$$h_2^2 - h_1^2 = \frac{Q}{\pi K} \ln\left(\frac{r_2}{r_1}\right) \tag{2}$$

where h is the hydraulic head in the piezometer $[L]$; Q is the pumping rate $[L^3/T]$; K is the hydraulic conductivity $[L/T]$; and r is the radial distance from the pumping well $[L]$.

Dupuit-Thiem's solution is based on the radial distribution of the drawdown and can therefore be applied to determine the spatial distribution of the reduction in hydraulic conductivity. The change in hydraulic conductivity is closely related to the reduction in permeability, due to the similarity in density and viscosity between the injected suspension and the groundwater (Zhou et al. 2019).

Due to the depth of the groundwater table and the narrow filter tubes [Fig. 1(a)], no pumping tests were performed in the upper wells. Instead, in selected upper wells (A/B 3, A7, and B10) constant-rate infiltration tests (infiltration rate around 25 m³/d) were performed before and after the injection. As reported by Payne et al. (2008), hydraulic equations used for pumping tests cannot provide accurate hydraulic characteristics under infiltration conditions. In this study, the results from the infiltration test are therefore only used qualitatively, to verify the results obtained from other data sets.

Groundwater sampling and analysis were performed at predefined well locations (A/B 2, 4, 5, 8, 9, and 10, and B11) on selected dates. Baseline measurements were performed in June, 2018. After the injection phase, groundwater sampling was performed on weekly basis for a month and continued with monthly monitoring for an additional six months. The samples were analyzed for total

organic carbon (TOC), Al (after filtration), chloride, and potassium (after filtration).

Site-Specific Flow Model

A site-specific flow model was implemented in COMSOL Multiphysics (v5.3) in order to design the installation of the flow barrier and to understand the impact of the changing hydraulic boundary conditions that are related to the dredging activities. Groundwater flow in the model is described by Darcy's law, and the governing equations are Richards' equation, combined with the extended version of Darcy's law:

$$\frac{\partial}{\partial t}(\varepsilon_p \rho S_w) + \nabla \cdot (\rho \mathbf{u}) = \rho Q_m \tag{3}$$

in which

$$\mathbf{u} = \frac{\mathbf{K} k_r(S_e)}{\mu} (\nabla p + \rho g \nabla z) \tag{4}$$

where t is time $[T]$; ρ is the fluid density $[M/L^3]$; S_w is the saturation degree $[L^3/L^3]$; $\mathbf{u}$ is the Darcy velocity $[L/T]$; Q_m is the volumetric source/sink term $[L^3/L^3T]$; k_r is the relative permeability $[-]$, which is a function of the effective saturation degree S_e, $[L^3/L^3]$; p is the pressure head $[L]$; μ is the dynamic viscosity of the fluid $[M/LT]$; g is the gravity acceleration constant $[L/T^2]$; and z is the vertical direction, assumed positive upwards $[L]$.

The model was used to simulate the hydraulic conditions in the profile shown in Fig. 1(a). The soil layering and corresponding transport properties were derived from site investigations and baseline pumping tests (before the injection of the Al-OM flocs). Input parameters used in the model are summarized in Table S1. The hydraulic boundaries (the water reservoir and the ditch) were implemented as Robin-type boundary conditions [Eq. (5)]:

$$\mathbf{u} = R_c(H_{ext} - H) \tag{5}$$

where H_{ext} is the known external hydraulic head $[L]$; H is the head at the boundary $[L]$; and R_c is the conductance term $[1/T]$.

© ASCE 04022095-6 J. Geotech. Geoenviron. Eng.

J. Geotech. Geoenviron. Eng., 2022, 148(11): 04022095

In this way, the entry resistance at the boundary can be denoted as the conductance term R_c. The conductance term was determined done by fitting against field monitoring data. The geometry, location, and permeability of the flow barrier were specified in the domain in the respective scenario analysis.

Results

Effect of the Direct Floc Injection on the Hydraulic Gradient

The presence of a continuous flow barrier can be identified by looking at changes in the hydraulic gradient before and after the direct Al-OM floc injection. The hydraulic gradient before the injection was determined by averaging the hydraulic head data that are monitored at all wells over a period of three months. The averaged hydraulic heads in Zones A and B are presented in Fig. 4. A nearly straight phreatic line is observed in both zones. The hydraulic gradients measured are relatively high, namely 0.05 and 0.028 m/m in Zones A and B, respectively. This is a consequence of the large difference between water levels in the water reservoir (6.5 m NAP) and the ditch (0.4 m NAP).

One month after the injection, the hydraulic gradient was again determined (over a period of three months) and distinct changes were observed. The one month waiting period was intended to minimize any lingering effect that the injected volume could have on the hydraulic field. The hydraulic head measured at all wells in Zone B increased by approximately 30 cm. The only exception is Well B7, where the measured head after the injection was abnormally high [Fig. 4(b)]. However, the evenly distributed increase in hydraulic head shows that the injection did not result in any change in the hydraulic gradient. It should be noted that the evenly distributed rise in the hydraulic head was also monitored at locations outside the testing area after the injection (data not shown).

A similar increase in the hydraulic head was measured in Zone A, but with variations in its magnitude depending on the location of the monitoring well. The increase in the hydraulic head at the wells which are the furthest downstream from the injection line (A8 and A9) is 20 cm less than at all other wells in Zone A [shown in Fig. 4(a)], where the increase in hydraulic head is around 35 cm. This result demonstrates that the hydraulic gradient between monitoring wells A6/7 and A8 became steeper after the injection, while it is comparable to the gradients measured before the injection

in the rest of the domain. This change in hydraulic gradient was consistently observed throughout the entire year after the injection (latest data was collected in the summer of 2019).

Hydraulic Characterization by Pumping and Infiltration Tests

In order to quantify the effect of the direct floc injection on the soil permeability, the spatial drawdown distributions during a pumping test performed before and after the injection were compared. Results from the pumping tests in Zones A and B before the injection (shown in Figs. 5 and 6) show a well shaped cone of depression, where the drawdown decreases with increasing radial distance from the pumping well. This indicates that the initial permeability of the two zones is rather homogeneous. The background hydraulic conductivity of Zones A and B was determined to be 6.3 and 7.6 m/d, respectively, using Dupuit-Thiem's solution [Eq. (2)]. As shown in Figs. 5 and 6, the calculated drawdown distribution using the background hydraulic conductivity matches the measured data very well.

After the injection the most profound difference in drawdown in Zone B was measured at Monitoring Wells B7 and B8. At these two locations the drawdown was significantly lower than at the other wells (Fig. 6). If Monitoring Points B7 and B8 are, however, excluded, the cone of depression after the injection is comparable to that measured before the injection in Zone B. Data obtained from Well B5 were considered as outliers because data monitored at this particular well location showed consistent discrepancies in tests performed before and after the injection.

The results from the pumping test in Well A9 show that the cone of depression in Zone A changed after the direct floc injection (Fig. 5): It is no longer uniformly distributed over the entire domain, but shows a distinct pattern change between Monitoring Wells A6/7 and A8. At Monitoring Wells A1-7 and A10, the pumping test performed after the injection led to a drawdown that is 6 cm less than before the injection. At Well A8, on the other hand, the drawdown increased by 4 cm. The change of measured drawdown across Wells A6/7 and A8 is consistent with the hydraulic gradient in this area [Fig. 4(a)].

The results from infiltration tests at various well locations before the injection (presented in Figs. S8 and S9) show that the magnitude of the head change primarily depends on the radial distance from the infiltration well. This corroborates the results from the pumping tests before the injection in Zone A and B. The same
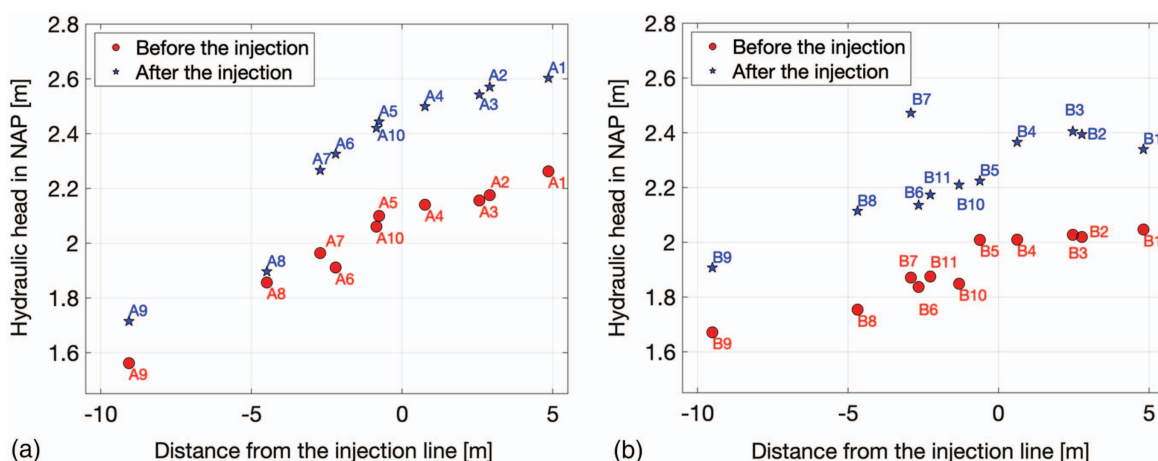
Fig. 4. (Color) Comparison of hydraulic gradient measured before and after the injection in (a) Zone A; and (b) Zone B.

© ASCE 04022095-7 J. Geotech. Geoenviron. Eng.

J. Geotech. Geoenviron. Eng., 2022, 148(11): 04022095
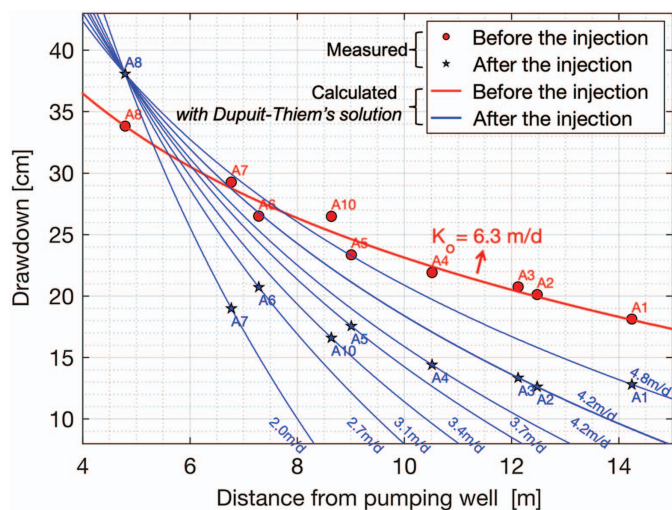
Fig. 5. (Color) Measured and calculated drawdown distribution from the pumping test performed in well A9 before and after the injection (pumping rate of 30 m³/d).
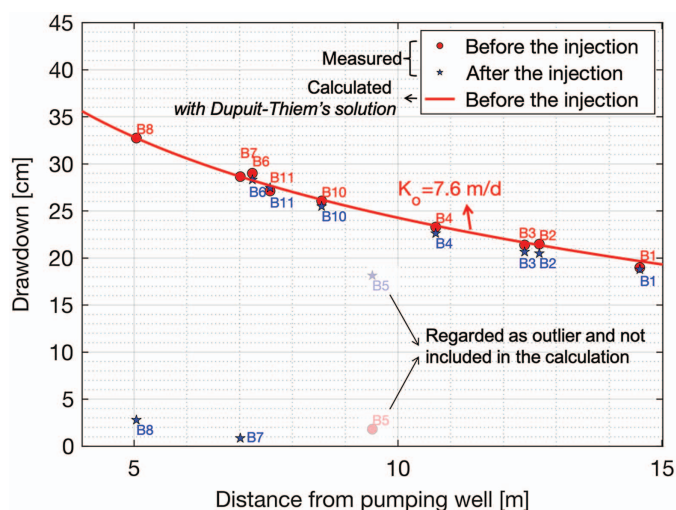
Fig. 6. (Color) Measured and calculated drawdown distribution from the pumping test performed in well B9 before and after the injection (pumping rate of 30 m³/d).

consistency when comparing infiltration and pumping tests is also found after the injection: In Zone A, the difference of measured head change between Wells A6/7 and A8 increased noticeably during the infiltration tests performed in Well A3 and A7 after the injection (Fig. S8). The difference between infiltration tests before and after the injection in Zone B is mainly identified at Monitoring Wells B7 and B8. The head change at these locations was considerably less than that measured in the test before the injection (Fig. S9).

Transport of the Injection Fluid

Continuous EC measurement in the monitoring wells allowed us to monitor the propagation of the injection fluid in the subsurface. It should be noted that the EC is mainly influenced by the concentrations of ions (Cl⁻ and K⁺) in the injected suspension. The transport of Al-OM flocs is not necessarily the same due to filtration and deposition.

In order to get an insight into the development of the injection [i.e., EC and change in head (dH)] in 2D space, interpolation was applied on scattered data monitored at well locations using Matlab (function scatteredInterpolant.m) and the interpolated results were used to generate topographies (Figs. 7 and S8–S10). Areas with limited confidence level, caused by the limited availability of scattered data, were shadowed. As shown in Figs. 7(a and b), the transport of the injection fluid in Zone B was subjected to preferential flow. Shortly after the start of the injection at Point I44, the EC value measured at Wells B7 and B8 significantly increased, to about 2.75 mS/cm. This corresponds with the EC of the injection fluid applied in this zone. At well locations in closer proximity to Injection Point I44 (Wells B5, B6, and B10) the increase in EC was much less pronounced, or even unnoticeable (Well B6). The change in hydraulic head is in line with the EC data [Figs. 7(c and d)]. The change in head measured at Wells B7 and B8 was so prominent that the linear interpolation (Fig. 7) suggests a large area with a significant increase in head. This cannot reflect the actual head in this area, because the injected volume is not enough to result in such a rise in water table over a large area. The EC data also revealed a down-gradient transport of the injection suspension. At Well B9, which is located approximately 10 m away from the injection line, the EC peaked at 2 mS/cm, while in the opposite direction (against the natural groundwater flow) only a gentle rise in EC was detected (the highest EC measured at Well B3 is 0.7 mS/cm). In Zone A (results presented in Fig. S10) a similar trend was observed: a preferential flow led first to a sharp rise of EC and dH at Well A8, followed by an increase at A6 and A7. In contrast to Zone B, no increase in EC at Well A9 was observed during the entire monitoring period.

Results from the chemical analysis of groundwater samples corroborate the field-measured EC data. Samples taken from Wells A8 and B8 on July 6, 2018 contained, respectively, 0.42 and 0.7 g/l of Cl⁻, and 0.25 and 0.44 g/l of K⁺. Both are comparable to that of the injection suspension used in the respective zones. The measured Al and TOC concentrations, however, were far lower. TOC concentrations of 19 and 60 mg/l were measured at Wells A8 and B8, which are higher than the background (around 5 mg/l) but not even close to the TOC concentrations in the injection suspension. Measured Al concentrations were consistently below 50 μg/l (detection limit), expect for one measurement in Well B8 directly after the injection, where a concentration of 400 μg/l was measured. This is again much lower than the Al concentration in the injection suspension.

Discussion

Permeability of the Flow Barrier in Zone A

The foregoing results all indicate that a flow barrier has been created in Zone A between Wells A6/7 and A8. The hydraulic gradient is noticeably steeper between Wells A6/7 and A8 even under ambient flow conditions. The head difference between those points increased from 10 cm before the injection to 37 cm after the injection (Fig. 4). This shows that the barrier is continuous throughout a relevant part of Zone A, because otherwise the measured signal would be less pronounced due to water bypassing the barrier, especially under steady state conditions (Cunningham and Reinhard 2002; Bayer et al. 2004; Anderson and Mesa 2006). The presence of the flow barrier is further confirmed by the results obtained from the pumping and infiltration tests. Literature shows that the presence of a flow barrier leads to distinct effects on either sides of the barrier during a pumping event (Bayer et al. 2004; Payne

© ASCE   04022095-8   J. Geotech. Geoenviron. Eng.

J. Geotech. Geoenviron. Eng., 2022, 148(11): 04022095
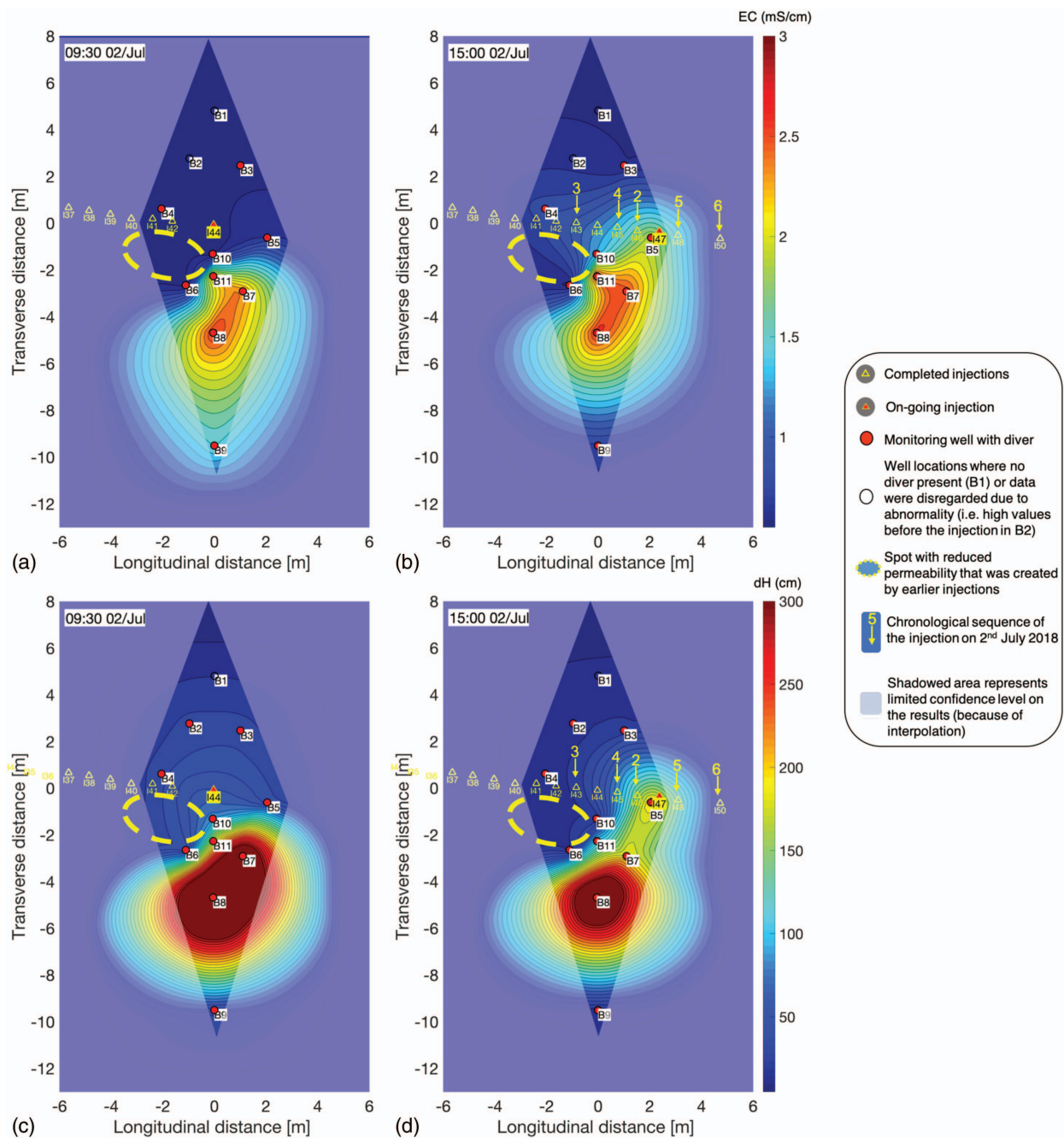
Fig. 7. (Color) Measured (a and b) EC; and (c and d) dH during the injection of the Al-OM flocs suspension. Figures (a) and (c) show the results at the end of the first injection in a day (I44); and (b) and (d) show the results at the end of the last injection of the day (I47).

et al. 2008; USEPA 2008). The low permeability of the flow barrier widens the capture zone of the pumping at the well. As a consequence a reduced discharge is observed at the side across the flow barrier, while at the side of the pumping well the discharge is locally enhanced (illustrated in Fig. S11). This is exactly what was observed during the pumping and infiltration tests in Zone A (described in the section "Hydraulic Characterization by Pumping and Infiltration Tests," and shown in Figs. 5 and S8).

We applied a hydraulic conductivity analysis to quantify the reduction in permeability of the flow barrier in Zone A. An equivalent hydraulic conductivity (K_{eq}) was derived from the pumping test results after the injection using Dupuit-Thiem's solution. The derivation of the equivalent hydraulic conductivity is based on measured drawdowns from two monitoring points at both sides of

the flow barrier (A8 and any other well downstream). The equivalent hydraulic conductivity is therefore an integrated hydraulic conductivity over (1) the area that is not affected by the injection of Al-OM flocs (with a background hydraulic conductivity K_o); and (2) the flow barrier itself (with a reduced hydraulic conductivity K_r). We assumed that the geometry of the flow barrier is linear with a sufficient lateral extension and that it extends over the entire saturated height of the aquifer. Consequently we calculated eight equivalent hydraulic conductivities in Zone A, which are presented in Fig. 5. It can be found that a larger distance between the two data points coincides with a larger K_{eq}. This is because a greater distance means that a larger proportion of unreduced hydraulic conductivity is integrated in the calculation of the respective K_{eq} (because the flow barrier is present between A6/7 and A8).

© ASCE   04022095-9   J. Geotech. Geoenviron. Eng.

J. Geotech. Geoenviron. Eng., 2022, 148(11): 04022095

The hydraulic conductivity of the flow barrier (K_r) is determined based on the assumption that the flow direction is perpendicular to the orientation of the flow barrier. Thus, the equivalent hydraulic conductivity is the harmonic mean (Renard and de Marsily 1997):

$$K_{eq} = \frac{\sum_{i=1}^{n} L_i}{\sum_{i=1}^{n}(L_i/K_i)} \tag{6}$$

where L_i is the thickness of layer i $[L]$; and K_i is the hydraulic conductivity of layer i $[L/T]$.

The average of all eight calculations was taken as the final hydraulic conductivity. One important variable that needs to be considered in this calculation is the thickness of the various layers. The flow barrier is located between Wells A6/7 and A8, which means that it is not thicker than 2 m. We therefore conducted a series of calculations assuming the thickness of the flow barrier to vary from 0.1 to 2 m. The corresponding hydraulic conductivity of the flow barrier is shown in Fig. S12. Based on the results, the effectiveness of the flow barrier is controlled by its thickness and its hydraulic conductivity. For example, a flow barrier with hydraulic conductivity of 0.6 m/d and a thickness of 1 m is as efficient in reducing groundwater flow as a barrier with a hydraulic conductivity of 0.15 m/d and a thickness of 0.2 m.

It should be noted that the hydraulic conductivity is vertically lumped over the saturated thickness of the treated dike body. As stated earlier, continuity, both planar and vertical, is essential to create an effective flow barrier. Based on available data, which came from sensors installed in the wells at a fixed depth, we cannot judge the vertical variability of the permeability in the flow barrier. For this reason, we assume that the Al-OM floc injection decreased the soil permeability homogeneously in the vertical direction. This implies that the factor of reduction calculated using the hydraulic conductivity is identical to that of the factor of permeability reduction (section "Monitoring and Data Analysis"). By assuming the thickness of the flow barrier created in Zone A matches the design (1 m), it can be concluded the direct floc injection reduced the permeability of the soil by 11 times. However, it should be noted that this quantification might considerably underestimate the true impact of the injected Al-OM flocs on soil permeability, because (a) the actual thickness of the flow barrier is highly uncertain, and (b) the Zone B (Fig. 6) and lab (Fig. 3) results clearly indicate that a significant reduction in soil permeability can be locally achieved. Results from our previous study (Zhou et al. 2019), on the other hand, showed that the flow barrier created by in-situ production of Al-OM flocs reduces soil permeability by a factor of 50. As a result, if the same reduction in permeability (i.e., by a factor of 50) is assumed, the flow barrier formed in Zone A would have a thickness of approximately 0.15 m, which is thinner than designed. This is also less effective than what is suggested by results from laboratory column experiments (Fig. 3).

Verification of the Quantification and the Impact of Dredging

The dredging activities had a significant impact on the field monitoring data. As indicated above, the hydraulic head measured at all well locations in the testing area (Zones A and B), as well as in neighboring areas, showed a noticeable increase after the field injection. This global elevation in hydraulic head was therefore not a consequence of the field injection (although the changed hydraulic gradient can be attributed to the injection); rather, it was the direct result of the dredging. The removal of the top soil reduced the resistance to water entering the soil body, and subsequently enhanced the discharge. Based on Darcy's law, the increased discharge rate in
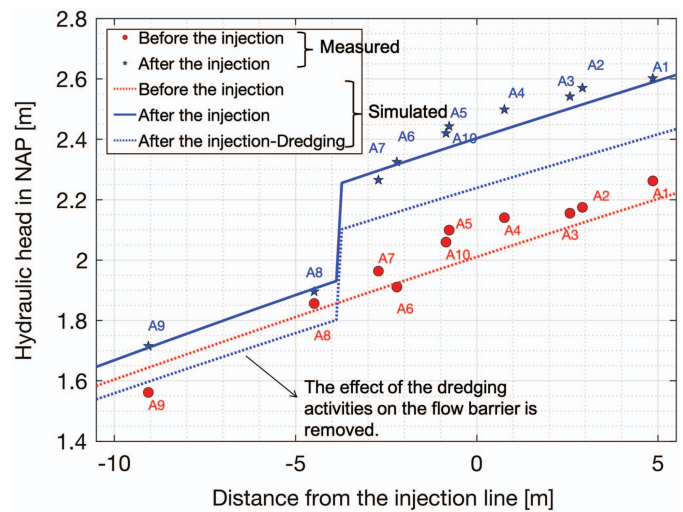
Fig. 8. (Color) Measured and simulated hydraulic gradient in Zone A, where circles and stars indicate measured data and the lines represent the simulated results of the site-specific flow model.

the soil body resulted in the observed rise in the hydraulic head on site. As such, the impact of the dreading activities can be considered as a change in hydraulic boundary condition. Verification of the analysis presented in the section "Permeability of the Flow Barrier in Zone A" was carried out with the site-specific flow model, which also takes into account the change in the hydraulic boundary condition after the injection, due to the dredging activities (detailed in the section "Site Description").

The initial conductance terms on both boundaries, i.e., the water reservoir and the ditch, were determined in the baseline scenario (before the injection) by calibrating against the phreatic line measured before the injection (Fig. 8). The conductance term assigned to the water reservoir boundary was increased for the analysis after the injection in order to account for the dredging. In addition, the flow barrier (assumed to be 0.15 m thick, with a permeability reduced 50 times, and located between Wells A6/7 and A8) was added to this scenario. Simulated results match the measured data well in both scenarios (shown in Fig. 8) and therefore provide credibility to the quantification described in the previous section. This analysis additionally confirms entry resistance in the water basin has been reduced and that, therefore, the dredging activities are the cause of the elevated groundwater table after the creation of the low permeability barrier.

A scenario analysis was constructed in order to remove the effects of the dredging activities. This was done by using the same conductance terms on both boundaries as in the baseline scenario for the situation after the injection. As shown in Fig. 8 (dashed blue line), the flow barrier in Zone A would have lowered the groundwater table at its downstream side by 5 cm if the dredging activities did not take place. The simulation results also indicate that the creation of the flow barrier would reduce the discharge from the water reservoir by approximately 3.5%, as the flow barrier provides additional resistance to the seepage flow that originates from the water reservoir. The reductions in the groundwater table and in the discharge would in that case both contribute to reduce the water content of the soil at the toe of the dike.

Localized Reduction in Permeability in Zone B

Although a rise in the hydraulic head was observed in all wells in Zone B after the injection [Fig. 4(b)], it was mostly attributed to the

© ASCE 04022095-10 J. Geotech. Geoenviron. Eng.

J. Geotech. Geoenviron. Eng., 2022, 148(11): 04022095

changed boundary condition caused by the dredging activities. There is little to no difference in the hydraulic gradient in Zone B after the injection, compared to before. This implies that no continuous flow barrier is created. There is, however, evidence of localized reductions in permeability. Both the pumping and the infiltration tests that were performed after the injection (Figs. 6 and S9) show that the hydraulic head at Wells B7 and B8 are hardly affected by the pumping/infiltration. Clearly, the permeability in the close vicinity of these wells was significantly reduced. The identification of this spot with reduced permeability is only possible because it is situated between the monitoring wells. The applied characterization methods (field pumping/infiltration tests) were designed to detect a continuous flow barrier. As discussed earlier, spot-wise reduction in permeability was very difficult to detect with our monitoring layout because of preferential flow paths, which bypass the low permeability zones. It is, therefore, possible that other spots with reduced permeability were created by the injection of Al-OM flocs, but those spots could not be detected with our monitoring layout.

Another spot with low permeability is located in between B6, B10, and B11 and the injection line (dashed yellow oval in Fig. 7). Tracking changes in EC during the injection of flocs provides an indirect method for detecting low permeability spots. Because a large concentration of chloride and potassium ions were co-injected with the flocs, it is possible to use changes in EC to estimate the transport pattern of the tracer, which provides insight into the soil permeability. A strong indication of preferential flow of the injection fluid is the immediate breakthrough of EC in Well A8 during injection in I7 and I13 (Fig. S10). Subsequently, a pronounced increase in EC was also measured at Wells A6 and A7. The injected suspension in Zone B, however, did not spread over Well B6. This is most likely the result of a reduced permeability in the area around B6 and B10 due to earlier injections (illustrated in Fig. 7). The low permeability of this spot diverted the injected suspension towards Well B7 and led to an asymmetric distribution of measured EC. Hydraulically, the change in head at this spot was also lower than at other locations, confirming the previous results [Figs. 7(c and d)]. A major difference between the low-permeability spot between Wells B7, B8, and B11, and the spot between B6, B10, and B11, is that the latter spot does not reach the various well locations. As such, the data that came out of these wells did not show distinct changes in hydraulic characterization after the injection, due to the occurrence of preferential flow via zones that were not affected by the injection, and thus had little or no deposition of Al-OM flocs.

Challenges in Process Control and Implementation

Occurrence of Preferential Flow

The flow barrier created in Zone A is located between Wells A6/7 and A8, which is 3 m further downstream than originally designed. This is partially attributed to the fact that the hydraulic gradient at this site is relatively high, leading to pore water velocities above 1 m/d (section "Effect of the Direct Floc Injection on the Hydraulic Gradient"). This forces the transport of flocs towards the downstream direction. There has to be, however, another transport mechanism that explains the preferential flow towards Monitoring Wells A8 and B8 (which are located 5 m away from the injection line). Full groundwater displacement cannot be the case, because the injected volume is far from sufficient to reach Well A8 or B8. Additionally no breakthrough was observed in other wells located closer to the injection line.

We hypothesize that the preferential flow is a combination of ambient groundwater flow, the installation of monitoring wells,

the creation of low-permeability zones in previous injections, and the occurrence of micro-hydraulic fracturing. Even though the wells were installed with a small diameter (OD 50 mm), the number of monitoring wells was relatively large. Compared with the flow of water in soil, the flow of water in a hollow tube is subjected to little resistance. This is particularly relevant when the flow rate is high (Pinder and Celia 2006; Chapuis and Chenaf 1998). Given the fact that the flow of water always follows the path of least resistance, the densely installed monitoring wells could have served as relief wells during the injection of Al-OM flocs, to which the flow was passively attracted (Chen et al. 2021). The ambient flow enhanced this effect towards the down-gradient side of the injection, which leads to a concentration of injection fluid downstream of the injection line. Hydraulic fracturing is initiated if the vertical effective stress of the soil is exceeded by the applied injection pressure (Payne et al. 2008; Luna et al. 2015). Among the down-gradient wells the lowest overburden pressure is found at the location of Wells A8 and B8. The vertical effective stress at Well A8 is nearly 10 kPa less than at Well A7 (i.e., $\sigma'_{v,A8} = 114.4$ kPa and $\sigma'_{v,A7} = 125.1$ kPa), which makes this location more prone to fracturing. The high injection pressure used was intended to ensure the spreading of Al-OM flocs, and it seems like this triggered micro-fracturing. Once a fracture channel is established, it will serve as the path of least resistance (Phillips et al. 2013). It has to be noted that there is no evidence of extensive fracturing or structural failure of the soil matrix, as the measured pressures during the injection indicated no sudden drop, and injection rates remained constant (Payne et al. 2008).

Production Recipe of Al-OM Flocs

The permeability reduction caused by the Al-OM flocs is the result of filtration and deposition, which takes place when the size of the flocs exceeds a certain threshold limit defined by the properties of the porous medium (Ryan and Elimelech 1996; Bradford et al. 2006; Xu et al. 2006; Molnar et al. 2015). This is confirmed by the difference between the TOC concentration and ion concentrations measured in Wells A8 and B8 (section "Transport of the Injection Fluid"), which indicates that most of the Al-OM flocs were filtered and immobilized along the transport path. Results from the lab experiments [Figs. 2(b) and 3] also revealed that the reduction in permeability can vary over a large range, depending on the amount of deposited Al-OM flocs. Therefore, in addition to the total mass of deposited flocs, their distribution in space is equally important in defining the overall effectiveness of the field injection. Ideally, an even distribution of deposited Al-OM flocs is preferred. This is because gaps within the flow barrier, or in other words spot-wise reductions in permeability, will lead to preferential flow.

Clearly, the input concentration plays a role in distributing the Al-OM flocs in-situ. A higher concentration corresponds to a larger probability for soil pores to be blocked by the flocs and thus a faster permeability reduction rate (Sharma and Yortsos 1987; Ryan and Elimelech 1996; Tosco and Sethi 2010). This corroborates with results from the column experiments, where injection was performed at different input OM concentrations (ranging from 0.1 to 5 g/l). For instance, when the input concentration increased from 3 to 5 g/l, the volume with significant floc deposition (based on a visual inspection of the color) decreased by approximately 32% at an injection velocity of 61.9 m/d. In regard to the field experiment, although more mass of Al-OM flocs was injected in Zone B than in Zone A, and the applied injection rate was kept at 60 m³/d in both zones (thus corresponding to no changes in the shear conditions), the distribution of deposited flocs in Zone B was less homogenous than in Zone A because the transport distance of the

© ASCE 04022095-11 J. Geotech. Geoenviron. Eng.

J. Geotech. Geoenviron. Eng., 2022, 148(11): 04022095

flocs became smaller with a higher input concentration. Also, the research by Yan et al. (2008) suggests that a high OM concentration leads to a faster regrowth rate of the Al-OM flocs, as well as larger floc sizes. Thus, the concentration applied in Zone B might be overly effective in reducing the soil permeability. In addition to a preferential flow, the high injected mass of Al-OM flocs clogged the soil along the transport path. As a result, the injected Al-OM flocs led to the creation in Zone B of localized spots with significantly reduced soil permeability (e.g., the spot around Wells B7 and B8). This was not the case in Zone A, where a lower injection concentration was applied. The achieved reduction in permeability is shown to be more continuous, which demonstrates that the injected Al-OM flocs had spread more widely. This suggests that a lower concentration favors the spreading of Al-OM flocs in-situ.

Besides the input concentration, a fundamental understanding of the breakage and regrowth kinetics of Al-OM flocs in porous media is essential to control their spatial distribution. Most of the available knowledge in the water treatment literature is derived from batch experiments (Duan and Gregory 2003; Wang et al. 2009; Yu et al. 2010), where the impacts of the interaction between Al-OM flocs and the soil matrix, as well as their transport, are not addressed. Results from the column experiments [shown in Figs. 3(a) and S2] indicate that low flow rates correspond to low shear conditions and more effective re-growth of injected flocs, which further reduces the soil permeability. The exact kinetics, however, remain unclear.

Comparison of the Results from Laboratory and Field Experiments

The processes occurring during field injection and during 1D column experiments are different in some important aspects. One of the differences lies in the flow conditions: a constant flow velocity in the 1D column versus a radially decreasing flow velocity field during field injection. The main consequence of this difference is that shear on the flocs is more or less constant in the 1D soil column, whereas in the field shear decreases non-linearly with radial distance. As floc sizes increase with decreasing shear, transport distances in the field become increasingly limited, and can only be controlled by the injection velocity.

Field injection experiments were carried out with a smaller amount of PV than in the 1D column experiments (1.1 PV on site and 10 PV in the lab), which was the reason for choosing relatively high concentrations (3 and 5 g/l in Zones A and B, respectively). This decision was based on a compromise. On the one hand we aimed for a process that ensures that pore throats are covered with flocs. From the 1D column experiments we concluded that the amount of injected Al-OM flocs did not have to be especially large to achieve this. On the other hand we needed a process that would have a short field injection duration, which can lower the cost of field implementation and thus make this technique more economically attractive.

A field site is three dimensional, and the heterogeneity of the natural soils has a profound impact on the spatial distribution of the injected flocs, but the impact of this heterogeneity cannot be assessed from 1D column experiments. It is therefore crucial to take these differences into account when interpreting the field injection results in view of the knowledge derived from lab experiments.

Conclusions

This is the first full-scale experiment in which direct Al-OM floc injection was applied to reduce soil permeability in-situ.

Field-measured data demonstrate that this approach is viable in reducing soil permeability and that a continuous flow barrier can be created in a dike body. The advantages of this approach are apparent. Direct-push injection requires no installation of injection wells, which is often a significant cost factor for large-scale applications (Suer et al. 2009). In addition, this approach relies only on a single component injection. The effort required to prepare and manage the injection solution on site is minimal. The field experiment demonstrated that the ease of field implementation and efficiency of this approach are both high, meaning that this newly developed approach is more friendly and economically feasible for large-scale applications.

Controlling the process in-situ is, however, challenging. Results from the laboratory column experiments and the field test clearly demonstrate that large (i.e., orders of magnitude) variations in permeability occur when applying direct Al-OM floc injection. The primary cause of these large variations lies in the distribution of deposited flocs in the porous medium. Also, as discussed earlier, continuity of the flow barrier is crucial. Ideally, the injected flocs should be homogeneously distributed over the target zone. Instead of providing the soil with large amount of flocs in a short period of time by injection (as was the case in Zone B), injection at a lower input concentration (i.e., 1 g/l) and in a larger volume of water is more favorable for improving the distribution of the deposited flocs. In addition, the spacing between two injections can be shortened, to provide an additional guarantee of the continuity of the flow barrier. Further development in monitoring strategy is needed, as well. Conventional monitoring approaches, such as the hydraulic head measured at wells, are quite valuable for testing the effectiveness of the flow barrier. However, these approaches rely heavily on the continuity of the flow barrier and provide little indication regarding the spatial distribution of the deposited flocs. New monitoring strategies need to be developed that can detect the spatial distribution of flocs in soils, preferably in a quantitative way. Shallow-depth geophysical measurements, such as electrical resistivity tomography (ERT) and electrical impedance spectrometry (EIS), have been studied as non-intrusive site investigation techniques for assessing the effectiveness of a flow barrier (Kemna et al. 2002; DeJong et al. 2013; Bryson et al. 2014; Paílková et al. 2017). Such methods often assume a relationship between electrical conductivity and water content (Bryson et al. 2014), or make use of the changes in bulk electrical conductivity caused by the injection of solutes (Kemna et al. 2002) to characterize the spatial distribution of the injected solution. The interpretation of field monitoring results can be improved if process-oriented forward model results are available. Further development in numerical modeling is needed, such as coupling the groundwater flow model to a reactive transport model. Also, it is desirable to differentiate the transport process of flocs, which can be better described with particle/colloid transport theory (Tosco and Sethi 2010), and the transport process of co-injected solutes, which is governed by advection and diffusion processes (van Wijngaarden et al. 2016).

Although challenges encountered in process control led to but limited success of this field experiment in Zone B, the results do demonstrate the versatility of this approach of direct Al-OM floc injection. The breakage and regrowth kinetics of Al-OM flocs are influenced by factors including the source and dosage of the Al, the source of the OM, and the applied injection method. With more detailed knowledge, we believe that the direct injection of Al-OM flocs has the potential to reduce permeability under a wide range of environmental conditions. Further laboratory and field studies are thus recommended in order to test the viability of this approach under different conditions.

© ASCE 04022095-12 J. Geotech. Geoenviron. Eng.

J. Geotech. Geoenviron. Eng., 2022, 148(11): 04022095

Data Availability Statement

All data, models, or code generated or used during the study are available in the 4TU.Centre for Research Data repository (https://researchdata.4tu.nl/), with DOI: 10.4121/uuid:3369bb46-50b8-4ab2-b5d2-f47cb9ae4380.

Supplemental Materials

Text S1, Table S1, and Figs. S1–S12 are available online in the ASCE Library (www.ascelibrary.org).

References

Anderson, E. I., and E. Mesa. 2006. "The effects of vertical barrier walls on the hydraulic control of contaminated groundwater." *Adv. Water Resour.* 29 (1): 89–98. https://doi.org/10.1016/j.advwatres.2005.05.005.

Bayer, P., M. Finkel, and G. Teutsch. 2004. "Combining pump-and-treat and physical barriers for contaminant plume control." *Ground Water* 42 (6): 856–867.

Blauw, M., J. W. M. Lambert, and M. N. Latil. 2009. "Biosealing: A method for in situ sealing of leakages." In Vol. 9 of *Proc., Int. Symp. on Ground Improvement Technologies and Case Histories, ISGI*, 125–130. Singapore: Research Publishing Services. https://doi.org/10.3850/GI132.

Bradford, S. A., J. Simunek, M. Bettahar, M. T. Van Genuchten, and S. R. Yates. 2006. "Significance of straining in colloid deposition: Evidence and implications." *Water Resour. Res.* 42 (12): 1–16. https://doi.org/10.1029/2005WR004791.

Bryson, L. S., R. Ortiz, and J. Leandre. 2014. "Effects of a grout curtain on hydraulic and electrical conductivity in a laboratory-scale seepage model." In *Proc., Geo-Congress 2014: Geo-characterization and Modeling for Sustainability*, Geotechnical Special Publication 234, edited by M. Abu-Farsakh, X. Yu, and L. R. Hoyos, 3233–3242. Reston, VA: ASCE. https://doi.org/10.1061/9780784413272.314.

Chapuis, R. P., and D. Chenaf. 1998. "Detecting a hydraulic short circuit along a monitoring well with the recovery curve of a pumping test in a confined aquifer: Method and example." *Can. Geotech. J.* 35 (5): 790–800. https://doi.org/10.1139/t98-046.

Chen, Y.-H., F. T.-C. Tsai, and N. H. Jafari. 2021. "Multiobjective optimization of relief well operations to improve levee safety." *J. Geotech. Geoenviron. Eng.* 147 (7): 04021041. https://doi.org/10.1061/(ASCE)GT.1943-5606.0002532.

Cunningham, J. A., and M. Reinhard. 2002. "Injection-extraction treatment well pairs: An alternative to permeable reactive barriers." *Ground Water* 40 (6): 599–607. https://doi.org/10.1111/j.1745-6584.2002.tb02546.x.

DeJong, J. T., et al. 2013. "Biogeochemical processes and geotechnical applications: Progress, opportunities and challenges." *Géotechnique* 63 (4): 287–301. https://doi.org/10.1680/geot.SIP13.P.017.

DeJong, J. T., B. M. Mortensen, B. C. Martinez, and D. C. Nelson. 2010. "Bio-mediated soil improvement." *Ecol. Eng.* 36 (2): 197–210. https://doi.org/10.1016/j.ecoleng.2008.12.029.

Duan, J., and J. Gregory. 2003. "Coagulation by hydrolysing metal salts." *Adv. Colloid Interface Sci.* 100–102 (Feb): 475–502. https://doi.org/10.1016/S0001-8686(02)00067-2.

Gomez, M. G., B. C. Martinez, J. T. DeJong, C. E. Hunt, L. A. deVlaming, D. W. Major, and S. M. Dworatzek. 2015. "Field-scale bio-cementation tests to improve sands." *Proc. Inst. Civ. Eng. Ground Improv.* 168 (3): 206–216. https://doi.org/10.1680/grim.13.00052.

Haouzi, F. Z., and B. Courcelles. 2018. "Major applications of MICP sand treatment at multi-scale levels: A review." In *Proc., 71st Canadian Geotechnical Conf. and 13th Joint CGS/IAH-CNC Groundwater Conf.* Richmond, VA, Canada: Canadian Geotechnical Society.

Hudak, P. F. 2001. "Locating groundwater monitoring wells near cutoff walls." *Adv. Environ. Res.* 5 (1): 23–29. https://doi.org/10.1016/S1093-0191(00)00038-1.

Ivanov, V., and J. Chu. 2008. "Applications of microorganisms to geotechnical engineering for bioclogging and biocementation of soil in situ." *Rev. Environ. Sci. Biotechnol.* 7 (2): 139–153. https://doi.org/10.1007/s11157-007-9126-3.

Jansen, B., K. G. J. Nierop, and J. M. Verstraten. 2002. "Influence of pH and metal/carbon ratios on soluble organic complexation of Fe(II), Fe(III) and Al(III) in soil solutions determined by diffusive gradients in thin films." *Anal. Chim. Acta* 454 (2): 259–270. https://doi.org/10.1016/S0003-2670(01)01551-3.

Jarvis, P., B. Jefferson, and S. A. Parsons. 2006. "Floc structural characteristics using conventional coagulation for a high doc, low alkalinity surface water source." *Water Res.* 40 (14): 2727–2737. https://doi.org/10.1016/j.watres.2006.04.024.

Kemna, A., J. Vanderborght, B. Kulessa, and H. Vereecken. 2002. "Imaging and characterisation of subsurface solute transport using electrical resistivity tomography (ERT) and equivalent transport models." *J. Hydrol.* 267 (3–4): 125–146. https://doi.org/10.1016/S0022-1694(02)00145-2.

Li, T., Z. Zhu, D. Wang, C. Yao, and H. Tang. 2006. "Characterization of floc size, strength and structure under various coagulation mechanisms." *Powder Technol.* 168 (2): 104–110. https://doi.org/10.1016/j.powtec.2006.07.003.

Luna, M., F. Gastone, T. Tosco, R. Sethi, M. Velimirovic, J. Gemoets, R. Muyshondt, H. Sapion, N. Klaas, and L. Bastiaens. 2015. "Pressure-controlled injection of guar gum stabilized microscale zerovalent iron for groundwater remediation." *J. Contam. Hydrol.* 181 (Oct): 46–58. https://doi.org/10.1016/j.jconhyd.2015.04.007.

Molnar, I. L., W. P. Johnson, J. I. Gerhard, C. S. Willson, and D. M. O'Carroll. 2015. "Predicting colloid transport through saturated porous media: A critical review." *Water Resour. Res.* 51 (9): 6804–6845. https://doi.org/10.1002/2015WR017318.

Mulligan, C. N., R. N. Yong, and B. F. Gibbs. 2001. "Remediation technologies for metal-contaminated soils and groundwater: An evaluation." *Eng. Geol.* 60 (1–4): 193–207. https://doi.org/10.1016/S0013-7952(00)00101-0.

Nikbakhtan, B., and M. Osanloo. 2009. "Effect of grout pressure and grout flow on soil physical and mechanical properties in jet grouting operations." *Int. J. Rock Mech. Min. Sci.* 46 (3): 498–505. https://doi.org/10.1016/j.ijrmms.2008.10.005.

Paílková, J., B. Gjunsburgs, Z. Zachoval, J. Veselý, and Z. Műnsterová. 2017. "Earth-fill dam monitored by EIS method during application of nutrient aqueous solution used in biosealing method." *IOP Conf. Ser.: Mater. Sci. Eng.* 251 (1): 012130. https://doi.org/10.1088/1757-899X/251/1/012130.

Papagianakis, A. T., and D. G. Fredlund. 1984. "A steady state model for flow in saturated-unsaturated soils." *Can. Geotech. J.* 21 (3): 419–430. https://doi.org/10.1139/t84-046.

Payne, F., J. Quinnan, and S. Potter. 2008. *Remediation hydraulics*. Boca Raton, FL: CRC Press.

Phillips, A. J., E. Lauchnor, J. J. Eldring, R. Esposito, A. C. Mitchell, R. Gerlach, A. B. Cunningham, and L. H. Spangler. 2013. "Potential CO_2 leakage reduction through biofilm-induced calcium carbonate precipitation." *Environ. Sci. Technol.* 47 (1): 142–149. https://doi.org/10.1021/es301294q.

Pinder, G. F., and M. A. Celia. 2006. *Subsurface hydrology*. New York: Wiley.

Proto, C. J., J. T. DeJong, and D. C. Nelson. 2016. "Biomediated permeability reduction of saturated sands." *J. Geotech. Geoenviron. Eng.* 142 (12): 04016073. https://doi.org/10.1061/(ASCE)GT.1943-5606.0001558.

© ASCE 04022095-13 J. Geotech. Geoenviron. Eng.

J. Geotech. Geoenviron. Eng., 2022, 148(11): 04022095

Renard, P., and G. de Marsily. 1997. "Calculating equivalent permeability: A review." *Adv. Water Resour.* 20 (5–6): 253–278. https://doi.org/10.1016/S0309-1708(96)00050-4.

Ryan, J. N., and M. Elimelech. 1996. "Colloid mobilization and transport in groundwater." *Colloids Surf., A* 107 (Feb): 1–56. https://doi.org/10.1016/0927-7757(95)03384-X.

Sauer, D., H. Sponagel, M. Sommer, L. Giani, R. Jahn, and K. Stahr. 2007. "Podzol: Soil of the year 2007. A review on its genesis, occurrence, and functions." *J. Plant Nutr. Soil Sci.* 170 (5): 581–597. https://doi.org/10.1002/jpln.200700135.

Scheel, T., L. Haumaier, R. H. Ellerbrock, J. Rühlmann, and K. Kalbitz. 2008. "Properties of organic matter precipitated from acidic forest soil solutions." *Org. Geochem.* 39 (10): 1439–1453. https://doi.org/10.1016/j.orggeochem.2008.06.007.

Sharma, M., and Y. Yortsos. 1987. "Transport of particulate suspensions in porous media: Model formulation." *AlChE J.* 33 (10): 1636–1643. https://doi.org/10.1002/aic.690331007.

Shen, L., Q. Du, H. Wang, W. Zhong, and Y. Yang. 2004. "*In situ* polymerization and characterization of polyamide-6/silica nanocomposites derived from water glass." *Polym. Int.* 53 (8): 1153–1160. https://doi.org/10.1002/pi.1520.

Suer, P., N. Hallberg, C. Carlsson, D. Bendz, and G. Holm. 2009. "Biogrouting compared to jet grouting: Environmental (LCA) and economical assessment." *J. Environ. Sci. Health Part A Toxic/Hazard. Subst. Environ. Eng.* 44 (4): 346–353. https://doi.org/10.1080/10934520802659679.

Syngouna, V. I., and C. V. Chrysikopoulos. 2012. "Transport of biocolloids in water saturated columns packed with sand: Effect of grain size and pore water velocity." *J. Contam. Hydrol.* 129–130 (3–4): 11–24. https://doi.org/10.1016/j.jconhyd.2012.01.010.

Tosco, T., M. Petrangeli Papini, C. Cruz Viggi, and R. Sethi. 2014. "Nanoscale zerovalent iron particles for groundwater remediation: A review." *J. Cleaner Prod.* 77 (Aug): 10–21. https://doi.org/10.1016/j.jclepro.2013.12.026.

Tosco, T., and R. Sethi. 2010. "Transport of non-Newtonian suspensions of highly concentrated micro- and nanoscale iron particles in porous media: A modeling approach." *Environ. Sci. Technol.* 44 (23): 9062–9068. https://doi.org/10.1021/es100868n.

USEPA. 2008. *A systematic approach for evaluation of capture zones at pump and treat systems*. Rep. No. EPA/600/R-08/003. Washington, DC: USEPA.

van Paassen, L. A. 2011. "Bio-mediated ground improvement: From laboratory experiment to pilot applications." In *Proc., Geo-Frontiers Congress 2011: Advances in Geotechnical Engineering*, Geotechnical Special Publication 211, edited by J. Han and D. E. Alzamora, 4099–4108. Reston, VA: ASCE.

van Wijngaarden, W. K., L. A. van Paassen, F. J. Vermolen, G. A. M. van Meurs, and C. Vuik. 2016. "A reactive transport model for biogrout compared to experimental data." *Transp. Porous Media* 111 (3): 627–648. https://doi.org/10.1007/s11242-015-0615-5.

Wang, X. C., P. K. Jin, and J. Gregory. 2002. "Structure of Al-humic flocs and their removal at slightly acidic and neutral pH." *Water Sci. Technol. Water Supply* 2 (2): 99–106. https://doi.org/10.2166/ws.2002.0051.

Wang, Y., B.-Y. Gao, X.-M. Xu, W.-Y. Xu, and G.-Y. Xu. 2009. "Characterization of floc size, strength and structure in various aluminum coagulants treatment." *J. Colloid Interface Sci.* 332 (2): 354–359. https://doi.org/10.1016/j.jcis.2009.01.002.

Wiesner, M. R., M. C. Grant, and S. R. Hutchins. 1996. "Reduced permeability in groundwater remediation systems: Role of mobilized colloids and injected chemicals." *Environ. Sci. Technol.* 30 (11): 3184–3191. https://doi.org/10.1021/es950784u.

Xu, S., B. Gao, and J. E. Saiers. 2006. "Straining of colloidal particles in saturated porous media." *Water Resour. Res.* 42 (12): 1–10. https://doi.org/10.1029/2006WR004948.

Yan, M., D. Wang, J. Ni, J. Qu, C. W. Chow, and H. Liu. 2008. "Mechanism of natural organic matter removal by polyaluminum chloride: Effect of coagulant particle size and hydrolysis kinetics." *Water Res.* 42 (13): 3361–3370. https://doi.org/10.1016/j.watres.2008.04.017.

Yihdego, Y. 2016. "Evaluation of flow reduction due to hydraulic barrier engineering structure: Case of urban area flood, contamination and pollution risk assessment." *Geotech. Geol. Eng.* 34 (5): 1643–1654. https://doi.org/10.1007/s10706-016-0071-1.

Yu, W.-Z., J. Gregory, and L. Campos. 2010. "Breakage and regrowth of Al-Humic flocs—Effect of additional coagulant dosage." *Environ. Sci. Technol.* 44 (16): 6371–6376. https://doi.org/10.1021/es1007627.

Zhao, Y. X., B. Y. Gao, H. K. Shon, B. C. Cao, and J.-H. Kim. 2011. "Coagulation characteristics of titanium (Ti) salt coagulant compared with aluminum (Al) and iron (Fe) salts." *J. Hazard. Mater.* 185 (2–3): 1536–1542. https://doi.org/10.1016/j.jhazmat.2010.10.084.

Zhou, J., S. Laumann, and T. J. Heimovaara. 2019. "Applying aluminum-organic matter precipitates to reduce soil permeability in-situ: A field and modeling study." *Sci. Total Environ.* 662 (Apr): 99–109. https://doi.org/10.1016/j.scitotenv.2019.01.109.

© ASCE   04022095-14   J. Geotech. Geoenviron. Eng.

J. Geotech. Geoenviron. Eng., 2022, 148(11): 04022095